Improved Adaptive Robust Control for Low Voltage Ride-Through of Front-End Speed Regulation Wind Turbine

HAIYING DONG[1,2], **NINGNING CHEN**[2], **XIAOQING LI**[2], **AND HONGWEI LI**[2]

[1]School of New Energy and Power Engineering, Lanzhou Jiaotong University, Lanzhou 730070, China
[2]School of Automation and Electrical Engineering, Lanzhou Jiaotong University, Lanzhou 730070, China

Corresponding author: Haiying Dong (hydong@mail.lzjtu.cn)

ABSTRACT This paper proposes a low voltage ride-through (LVRT) control method for the front-end speed regulation (FESR) wind turbine based on an improved adaptive robust control (IARC) to find the solution of the generator parameter variation by grid voltage dip and enhance the LVRT capability of the FESR. First, the FESR system mathematical models and the control objective of LVRT are analyzed. Then, in the improved adaptive robust controller, the Lyapunov function for three sub-systems and the energy function of the system are constructed. The excitation control law and parameter replacement law of the system are obtained by the error compensation term and additional control variable. The method makes the energy function satisfy the dissipation inequalities to guarantee the stability and ability to suppress disturbance of the system. To verify the effectiveness of the proposed control method, the proposed IARC is compared with the predictive fuzzy PID (PFPID) by time-domain simulations under different fault conditions. The results show that the proposed IARC can not only realize the rapid regulation of reactive power and effective resistance to grid voltage fluctuations but also improve robustness and transient stability of the system and enhance the LVRT performance of the FESR during the grid voltage dip.

INDEX TERMS Front-end speed regulation (FESR) wind turbine, grid voltage dip, low voltage ride-through, adaptive robust control.

I. INTRODUCTION

The wind power capacity in the proportion of total energy power systems is increasing [1]–[4], which might bring great challenges to the safe and stable operation of the power grid [5]–[8]. To improve the reliability of the power system, the wind turbine should remain connected to the grid during the grid voltage dip. In other words, the wind turbine connected to the power grid must have low voltage ride-through (LVRT) capability [9]–[12].

When a three-phase short-circuit fault occurs in the power system, the voltage at PCC is dropped due to the grid faults and will result in a high short-circuit current in the stator windings. Meanwhile, the electromagnetic power is reduced which will cause the imbalance of the mechanical power to the generator and the electromagnetic power. The rotor

The associate editor coordinating the review of this manuscript and approving it for publication was Mou Chen.

speed of the generator will increase and affect the stability of the front-end speed regulation (FESR) wind turbine. When an asymmetric fault occurs in the power system, besides the above mentioned in the symmetrical fault, the magnetic coupling between the stator and rotor circuit causes higher harmonics in the stator and rotor windings [13]. Therefore, it is necessary to propose a control method to enhance the stability and the LVRT performance of FESR during grid asymmetrical and asymmetrical faults.

In [14], the LVRT performance of the FESR was analyzed in the DIgSILENT. Reference [15] designed a field voltage controller under different operation conditions including faults, and the controller can guarantee the characteristics of reactive power control and dynamical stability control for the FESR. In [16], the grid-connected stability and the fault ride-through capability were analyzed by a single machine model of the 2MW FESR. Reference [17] proposed an LVRT control method based on the working principles of the FESR,

the LVRT dynamic characteristics of the FESR are simulated during the power grid fault, and simulation results show that the proposed control method is effective. The above literature has achieved certain control effects for the LVRT control of the FESR. However, when the grid voltage dip, on the one hand, the mechanical power of the generator decreased, which results in excess power. On the other hand, the saturated extent of the magnetic circuit of the generator will change due to the grid fault, which results in the variation of the generator parameter. The generator parameter variation might increase the difficulty of the LVRT. However, none of the above literature mentions it.

Therefore, the external disturbance and the uncertainty of the generator parameter should be considered when designing an excitation controller to ensure the FESR connecting to the power grid during faults. Some of the excitation control methods such as direct-feedback linearization, sliding-mode control, robust sliding-mode control, Hamiltonian energy function, L_2 gain disturbance attenuation, nonlinear adaptive control are suggested for the synchronous generator [18]–[23]. However, the adaptive control method has advantages in dealing with parameter uncertainty. Reference [24]–[26] designed an excitation controller based on the adaptive back-stepping method, which can guarantee the stability of the system. Combining the adaptive back-stepping and sliding mode control, the authors designed an adaptive back-stepping sliding mode controller [27]. In [28]–[30], an improved adaptive back-stepping method was proposed based on error compensation, which can ensure the stability of the system and achieve real-time parameter estimation. To simplify the calculation and improve the convergence speed of the control variables, an improved nonlinear adaptive L_2 gain control was proposed by adopting the additional control variable and K class functions in the design process of the controller [31]. Reference [32] proposed a control method by modifying the traditional back-stepping adaptive L_2 gain control algorithm and linear matrix inequality, which can improve the dynamic stability of the system. In [33], a robust adaptive back-stepping method was proposed based on the higher-order dynamical models of synchronous generators and the simulation proved the feasibility and superiority of the proposed control method. Considering the uncertainty in the parameter of the excitation system model, the optimal robust excitation controller was designed in [34].

Based on the points discussed above, this paper proposed an LVRT control method for the FESR based on adaptive back-stepping and L_2 gain control. The new contribution of this paper can be summarized as below:

First, the variation of the generator parameter caused by grid voltage dips was considered in the method, so that the proposed control method has advantages in insensitivity to disturbance and parameters changes.

Then, the error compensation term and additional control variable were used when designing the controller, which can realize the rapid regulation of reactive power and effective

resistance to grid voltage fluctuations, suppress the oscillation better and improve the response speed of the system.

This paper is organized as follows. The brief review of the LVRT control method of the FESR in section 1. In section 2, the system modeling and the control objective are introduced. An improved adaptive robust excitation controller is designed in section 3. In section 4, the simulations are carried out under the grid symmetrical and unsymmetrical fault conditions to demonstrate the proposed method. The conclusions of this paper are given in section 5.

II. SYSTEM MODELLING AND CONTROL OBJECTIVE
A. SYSTEM MODELLING
As shown in Fig.1, the developed FESR is composed of five parts: wind turbine, main gearbox, windrive and brushless electric excitation synchronous generator (EESG) [35], [36]. The wind turbine converts the absorbed wind energy into mechanical energy and transmits it to the main gearbox. Then, the main gearbox converts the low speed of the wind turbine into a high speed that meets the requirements for windrive. The windrive uses a hydraulic torque flexible drive with flexible transmission performance to adjust the speed. The EESG is directly connected to the grid to replace the converter in the traditional wind turbine, which makes the FESR has larger reactive power compensation, better power quality, and higher reliability.
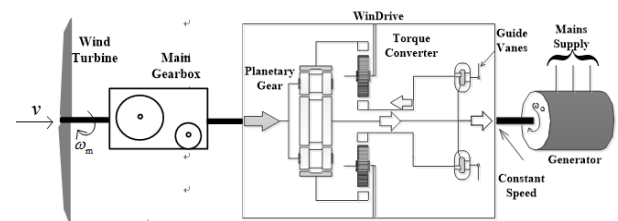

FIGURE 1. Structure of the FESR.

1) WIND TURBINE MODELLING
According to the aerodynamic principle, the relationship between the wind speed and the power extraction of the wind turbine is expressed by the following equation [37]–[40]

$$P_{\mathrm{M}} = \frac{1}{2}\rho\pi C_{\mathrm{p}}(\lambda, \beta)R^2 v^3 \qquad (1)$$

where P_{M} is the extracted power of the wind turbine, ρ is the air density, C_{p} is the power coefficient, λ is the tip speed ratio, β is the pitch angle, R is the radius of the wind rotor, v is the wind speed.

The wind power extracted by a wind turbine depends on the power coefficient $C_{\mathrm{p}}(\lambda, \beta)$, which is a function of both the tip speed ratio (λ) and the blade pitch angle (β). The tip speed is expressed as

$$\lambda = R\omega_{\mathrm{R}}/v \qquad (2)$$

where ω_{R} is the rotating speed of the blades.

FIGURE 2. The dynamic model of the drive system.

FIGURE 3. Configuration of a single-machine system.
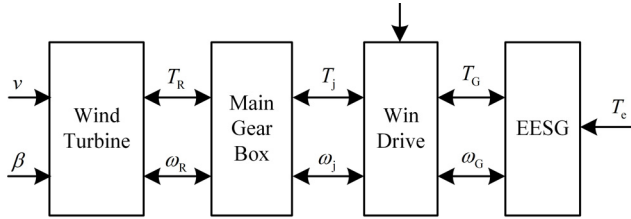
$C_p(\lambda, \beta)$ can be calculated by the following approximation equation

$$C_P(\lambda, \beta) = 0.5176\left(\frac{116}{\lambda_i} - 0.4\beta - 5\right)\exp\left(\frac{-21}{\lambda_i}\right) + 0.0068\lambda \tag{3}$$

The relationship between the extracted power P_M and the mechanical torque of wind turbine T_R is

$$P_M = T_R\omega_R \tag{4}$$

2) DRIVE SYSTEMS MODELLING

The dynamic model of the drive system is shown in Fig. 2. The characteristic of the wind turbine rotor and the low-speed shaft is described by using a simple mass-damping model as follows

$$J_R\frac{d\omega_R}{dt} = T_R - T_j - D_Z\omega_R \tag{5}$$

where J_R is the moment of inertia of the turbine rotor, T_j is the output torque of the main gearbox, D_Z is the damping coefficient of the low-speed shaft.

Ignoring the moment of inertia of the main gearbox, the following characteristics are obtained by the equation

$$\begin{cases} \omega_j = \omega_R i_{Rj} \\ T_j = \dfrac{T_R\omega_R}{\omega_j\eta_1} \end{cases} \tag{6}$$

where ω_j is the output speed of the main gearbox, i_{Rj} is the speed increase ratio of the main gearbox, η_1 is the transmission efficiency of the main gearbox.

In windrive, the dynamic balance equations between the pump shaft and the turbine shaft are given by

$$\begin{cases} J_t\dfrac{d\omega_P}{dt} = T_t - T_P - T_G \\ J_q\dfrac{d\omega_T}{dt} = T_q - T_T \end{cases} \tag{7}$$

where J_t is the moment of inertia of the sun gear, J_q is the moment of inertia of the outer gear ring, ω_p is the speed of the pump wheel, ω_T is the speed of the turbine wheel, T_p is the torque of the pump wheel, T_t is the torque of the sun gear, T_G is the input torque of the EESG, T_q is the torque of the outer gear ring, T_T is the torque of the turbine wheel.
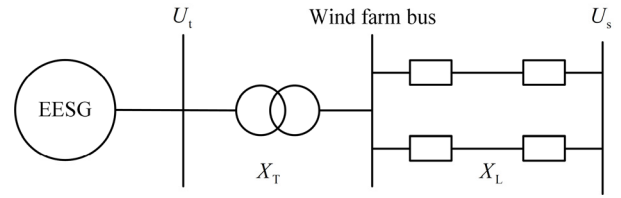
The relationship of the rotating speed of the blades, the pump wheel speed and the turbine wheel speed are given by

$$\frac{d\omega_T}{dt} = \frac{1 + i_{Tq}}{1 + i_{tq}}\left(\frac{d\omega_p}{dt} - i_{Rj} \cdot i_{tq} \cdot \frac{d\omega_R}{dt}\right) \tag{8}$$

where i_{Tq} is the speed ratio between the turbine wheel and the outer gear ring, i_{tq} is the speed ratio between the sun gear and the outer gear ring.

Ignoring the moment of inertia of the high-speed shaft, the characteristic of the generator rotor and the high-speed shaft is described as

$$\begin{cases} \dfrac{d\delta}{dt} = \omega_G \\ J_G\dfrac{d\omega_G}{dt} = T_e - T_G - D_G\omega_G \end{cases} \tag{9}$$

where δ is the power angle of the generator, ω_G is the speed of the generator, J_G is the moment of inertia of the generator rotor, T_e is the electromagnetic torque, D_G is the damping coefficient of the high-speed shaft.

3) EESG MODELLING

The EESG is connected to the grid through a step-up transformer and a dual-circuit transmission line. The configuration of the single-machine system is shown in Fig. 3.

The third-order models of the generator with perturbations are as shown in (10) to (12).

$$\dot{\delta} = \omega_G - \omega_0 \tag{10}$$

where ω_0 is generator speed at steady state.

$$\dot{\omega}_G = \frac{\omega_0}{H}P_T - \frac{D_G}{H}(\omega_G - \omega_0) - \frac{\omega_0}{H}\frac{E_q'U_s\sin\delta}{X_{d\Sigma}'} + w_1 \tag{11}$$

where H is the moment of inertia; P_T is the output power of the windrive; E_q' is the quadrature axis transient voltage of the generator; $X_{d\Sigma}' = X_d' + X_T + X_L$, X_d', X_T and X_L are the direct axis transient reactance of the generator, the reactance of the transformer, and the line reactance, respectively; U_s is the infinite bus voltage; w_1 is torque interference on the rotating shaft of the generator.

$$\dot{E}_q' = -\frac{1}{T_d'}E_q' + \frac{X_d - X_d'}{X_{d\Sigma}'T_{d0}}U_s\cos\delta + \frac{1}{T_{d0}}E_f + w_2 \tag{12}$$

where $T_d' = T_{d0}X_d'/X_d$, X_d is direct axis steady reactance of the generator, T_d' is the direct axis transient time

constant, T_{d0} is the time constants of excitation winding, E_f is excitation voltage, w_2 is electromagnetic interference of the generator excitation winding.

B. CONTROL OBJECTIVE

When the grid voltage dip, the saturation extent of the magnetic circuit of the generator will change, and the generator parameter will change according to the variations in the saturation extent. Therefore, the generator parameter is uncertain. Let $\theta = -D_G/H$.

$(\delta_0, \omega_0, E_{q0'})$ is the steady-state working point of the system. Define the system state variables as $x_1 = \delta - \delta_0$, $x_2 = \omega_G - \omega_0$, $x_3 = E'_q - E'_{q0}$.

Considering the influence of the generator parameter uncertainty and interference, the mathematical model of the EESG can be written as

$$\begin{cases} \dot{x}_1 = x_2 \\ \dot{x}_2 = \theta x_2 + k_0 P_T - k_1 \sin(x_1 + \delta_0)(x_3 + E'_{q0}) + w_1 \\ \dot{x}_3 = -\frac{1}{T'_d}(x_3 + E'_{q0}) + k_2 \cos(x_1 + \delta_0) + \frac{1}{T_{d0}}E_f + w_2 \end{cases} \quad (13)$$

where $k_0 = \frac{\omega_0}{H}$, $k_1 = \frac{\omega_0}{H}\frac{U_s}{X'_{d\Sigma}}$, $k_2 = \frac{X_d - X'_d}{X'_{d\Sigma}T_{d0}}U_s$.

The regulated output is given by

$$\mathbf{y} = \begin{bmatrix} q_1 x_1 \\ q_2 x_2 \end{bmatrix}$$

where $\mathbf{y}$ is evaluation signal; quantities q_1 and q_2 are nonnegative weighted coefficients, representing the weighted proportion of state variables x_1 and x_2 into the system output, which are to be determined by the designer in each particular case study. They satisfy the constraints: $q_1 + q_2 = 1$, $q_1^2 + q_2^2 \le 1$, $q_1 > 0$, $q_2 > 0$ [28].

To realize the low voltage ride-through control of the FESR, for any given $\gamma > 0$, design an excitation controller E_f and positive storage function $V(\mathbf{x})$ such that the following dissipation inequality holds for any final time $t > 0$: $V(x(t) - x(0)) \le \int_0^t (\gamma^2 ||\mathbf{w}||^2 - ||\mathbf{y}||^2)dt$.

And when $\mathbf{w}_1 = 0$, $\mathbf{w}_2 = 0$, the closed-loop system is asymptotically stable at $x = 0$. Then the L_2 gain from the disturbance to the output of the system is smaller than or equal to γ, where γ is disturbance attenuation constant.

III. LVRT METHOD BASED ON ADAPTIVE ROBUST EXCITATION CONTROL

A. DESIGN OF ADAPTIVE ROBUST EXCITATION CONTROLLER

Step 1: For the first subsystem of system (13), x_2 is assumed to be the virtual control variable. Define error variable $e_1 = x_1$, $e_2 = x_2 - x_2^*$, choose the virtual control of x_2 as: $x_2^* = -c_1 e_1 - p_1 e_2$.

where $c_1 > 0$ is a design parameter, $p_1 > 0$ is the error compensation coefficient, $p_1 e_2$ is an error compensation to compensate for the dynamic impact of the unknown error in the stabilization process.

While noting that

$$\dot{e}_2 = \frac{1}{(1 - p_1)} \left[\theta x_2 + k_0 P_T - k_1 \sin(x_1 + \delta_0)(x_3 + E'_{q0}) \right. \\ \left. + w_1 + c_1 x_2 \right] \quad (14)$$

For the first subsystem of system (13), define a Lyapunov function as follows

$$V_1 = \frac{e_1^2}{2}$$

The derivative of V_1 is written as

$$\dot{V}_1 = e_1 \dot{e}_1 = -c_1 e_1^2 + (1 - p_1)e_1 e_2$$

Step 2: For the (x_1, x_2) subsystem of system (13), x_3 is assumed to be the virtual control variable. Define error variable $e_3 = x_3 - x_3^*$, x_3^* is the virtual control of x_3. For this subsystem, define a Lyapunov function as

$$\dot{V}_2 = \dot{V}_1 + e_2 \dot{e}_2 = -c_1 e_1^2 + (1 - p_1)e_1 e_2 \\ + \frac{e_2}{1 - p_1}\left[\theta x_2 + k_0 P_T - k_1 \sin(x_1 + \delta_0)(x_3 + E'_{q0}) \right. \\ \left. + w_1 + c_1 x_2 \right] \quad (15)$$

And the further result is

$$x_3^* = \frac{(1 - p_1)^2 e_1 + \hat{\theta}x_2 + k_0 P_T + c_1 x_2 + c_2 e_2}{k_1 \sin(x_1 + \delta_0)} - E'_{q0} - p_2 e_3 \quad (16)$$

where $c_2 > 0$ is a design parameter, $p_2 > 0$ is the error compensation coefficient, $p_2 e_3$ is the error compensation term, which compensates for the dynamic impact of the unknown error in the stabilization process. $\hat{\theta}$ is the estimate of θ, $\tilde{\theta}$ is the estimated error and $\tilde{\theta} = \theta - \hat{\theta}$.

Substituting (16) into (15), it can be obtained

$$\dot{V}_2 = -c_1 e_1^2 + \frac{e_2 w_1}{1 - p_1} - \frac{c_2 e_2^2}{1 - p_1} \\ + \frac{e_2}{1 - p_1}[\tilde{\theta}x_2 - k_1 \sin(x_1 + \delta_0)(1 - p_2)e_3] \quad (17)$$

Then, take the derivative of e_3

$$\dot{e}_3 \\ = \frac{1}{1 - p_2}\{ -\frac{1}{T'_d}(x_3 + E'_{q0}) + k_2 \cos(x_1 + \delta_0) + \frac{1}{T_{d0}}E_f \\ + w_2 - \frac{[(1 - p_1)^2 x_2 + \dot{\hat{\theta}}x_2 + \frac{c_1 c_2 x_2}{1 - p_1}]}{k_1 \sin(x_1 + \delta_0)} \\ - \frac{(\hat{\theta} + c_1 + \frac{c_2}{1 - p_1})[\theta x_2 + k_0 P_m - k_1 \sin(x_1 + \delta_0)(x_3 + E'_{q0}) + w_1]}{k_1 \sin(x_1 + \delta_0)} \\ + \frac{[(1 - p_1)^2 e_1 + \hat{\theta}x_2 + k_0 P_T + c_1 x_2 + c_2 e_2]k_1 x_2 \cos(x_1 + \delta_0)}{k_1^2 \sin^2(x_1 + \delta_0)} \} \quad (18)$$

Step 3: For the (13), the global Lyapunov function is

$$V_3 = V_2 + \frac{1}{2}f(e_3)^2 + \frac{1}{2\rho}\tilde{\theta}^2$$

The derivative of V_3 is described as

$$\dot{V}_3 = \dot{V}_2 + f(e_3)\frac{df(e_3)}{de_3}\dot{e}_3 + \frac{1}{\rho}\tilde{\theta}\dot{\tilde{\theta}}$$

$$= -c_1 e_1^2 + \frac{e_2 w_1}{1-p_1} - \frac{c_2 e_2^2}{1-p_1} + f(e_3)\frac{df(e_3)}{de_3}\dot{e}_3$$

$$+ \frac{e_2}{1-p_1}[\tilde{\theta}x_2 - k_1\sin(x_1+\delta_0)(1-p_2)e_3] + \frac{1}{\rho}\tilde{\theta}\dot{\tilde{\theta}} \tag{19}$$

Substituting (18) into (9), let $b_3 = f(e_3)\frac{df(e_3)}{de_3}$, it holds that

$$\dot{V}_3$$
$$= \dot{V}_2 + b_3\dot{e}_3 + \frac{1}{\rho}\tilde{\theta}\dot{\tilde{\theta}} = \dot{V}_2$$

$$= -c_1 e_1^2 - \frac{c_2 e_2^2}{1-p_1} + \frac{e_2 w_1}{1-p_1} + \frac{b_3 w_2}{1-p_2}$$

$$- \frac{1}{1-p_2}\frac{(\hat{\theta}+c_1+\frac{c_2}{1-p_1})w_1}{k_1\sin(x_1+\delta_0)} + \frac{e_2}{1-p_1}\tilde{\theta}x_2$$

$$- \frac{1}{1-p_2}\frac{(\hat{\theta}+c_1+\frac{c_2}{1-p_1})\tilde{\theta}x_2}{k_1\sin(x_1+\delta_0)}$$

$$+ \frac{1}{\rho}\tilde{\theta}\dot{\tilde{\theta}} - \frac{e_2}{1-p_1}k_1\sin(x_1+\delta_0)(1-p_2)b_3$$

$$+ b_1\{-\frac{1}{T_d'}(x_3+E_{q0}')$$

$$+ k_2\cos(x_1+\delta_0) + \frac{1}{T_{d0}}E_f - \frac{[(1-p_1)^2 x_2 + \dot{\hat{\theta}}x_2 + \frac{c_1 c_2 x_2}{1-p_1}]}{k_1\sin(x_1+\delta_0)}$$

$$- \frac{(\hat{\theta}+c_1+\frac{c_2}{1-p_1})[\hat{\theta}x_2 + k_0 P_T - k_1\sin(x_1+\delta_0)(x_3+E_{q0}')]}{k_1\sin(x_1+\delta_0)}$$

$$+ \frac{[(1-p_1)^2 e_1 + \hat{\theta}x_2 + k_0 P_T + c_1 x_2 + c_2 e_2]k_1 x_2\cos(x_1+\delta_0)}{k_1^2\sin^2(x_1+\delta_0)}\} \tag{20}$$

where $f(e_3) = 2|e_3| + \cos e_3$, $\rho > 0$ is the adaptive gain coefficient.

Then, the parameter replacement law can be given by

$$\dot{\hat{\theta}} = \rho[-\frac{e_2}{1-p_1} + \frac{1}{1-p_2}\frac{(\hat{\theta}+c_1+\frac{c_2}{1-p_1})}{k_1\sin(x_1+\delta_0)}]x_2 \tag{21}$$

The excitation control law is selected as

$$E_f$$
$$= T_{d0}\{\frac{e_2}{1-p_1}k_1\sin(x_1+\delta_0)(1-p_2)^2 + \frac{1}{T_d'}(x_3+E_{q0}')$$

$$- k_2\cos(x_1+\delta_0) + \frac{[(1-p_1)^2 x_2 + \dot{\hat{\theta}}x_2 + \frac{c_1 c_2 x_2}{1-p_1}]}{k_1\sin(x_1+\delta_0)}$$

$$+ \frac{(\hat{\theta}+c_1+\frac{c_2}{1-p_1})[\hat{\theta}x_2 + k_0 P_T - k_1\sin(x_1+\delta_0)(x_3+E_{q0}')]}{k_1\sin(x_1+\delta_0)}$$

$$- \frac{[(1-p_1)^2 e_1 + \hat{\theta}x_2 + k_0 P_T + c_1 x_2 + c_2 e_2]k_1 x_2\cos(x_1+\delta_0)}{k_1^2\sin^2(x_1+\delta_0)}$$

$$- c_3 b_3 - u_f\} \tag{22}$$

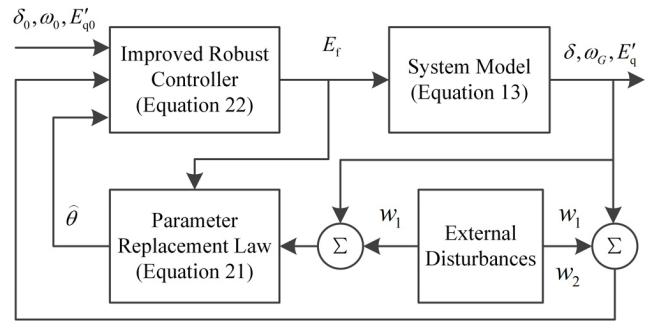**FIGURE 4.** The block diagram of the improved robust controller.

Substituting (21) and (22) into (20), it holds that

$$\dot{V}_3 = -c_1 e_1^2 - \frac{c_2 e_2^2}{1-p_1} - \frac{c_3 b_3^2}{1-p_2} + \frac{e_2 w_1}{1-p_1} + \frac{b_3 w_2}{1-p_2}$$

$$- \frac{1}{1-p_2}\frac{(\hat{\theta}+c_1+\frac{c_2}{1-p_1})w_1}{k_1\sin(x_1+\delta_0)} - \frac{b_3 u_f}{1-p_2} \tag{23}$$

where $c_3 > 0$ is a design parameter, u_f is an additional control variable.

Considering (23), the function is defined as

$$H = \dot{V}_3 + \frac{1}{2}(||y||^2 - \gamma^2||w_1||^2 - \gamma^2||w_2||^2) \tag{24}$$

Substituting (23) into H, it can be expressed as

$$H$$
$$= -c_1 e_1^2 - \frac{c_2 e_2^2}{1-p_1} - \frac{c_3 b_3^2}{1-p_2} + \frac{q_1^2 x_1^2 + q_2^2 x_2^2}{2} - \frac{b_3}{1-p_2}u_f$$

$$- [\frac{\gamma w_1}{\sqrt{2}} - \frac{(\hat{\theta}+c_1+c_2/1-p_1)w_1/(1-p_2)k_1\sin(x_1+\delta_0)}{\sqrt{2}\gamma}]^2$$

$$+ \frac{[(\hat{\theta}+c_1+c_2/1-p_1)w_1/(1-p_2)k_1\sin(x_1+\delta_0)]^2}{2\gamma^2}$$

$$- [\frac{\gamma w_2}{\sqrt{2}} - \frac{b_3/(1-p_2)}{\sqrt{2}\gamma}]^2 + \frac{[b_3/(1-p_2)]^2}{2\gamma^2} \tag{25}$$

Considering (25), the additional control u_f is expressed as:

$$u_f = \frac{1-p_2}{b_3}\{\frac{[(\hat{\theta}+c_1+c_2/1-p_1)w_1/(1-p_2)k_1\sin(x_1+\delta_0)]^2}{2\gamma^2}$$

$$+ \frac{[b_3/(1-p_2)]^2}{2\gamma^2} + \frac{q_1^2 x_1^2 + q_2^2 x_2^2}{2}\} \tag{26}$$

Thus, the excitation control law and parameter replacement laws are designed to guarantee the stability of the whole system. The block diagram of the designed controller is shown in Fig. 4.

B. PROOF OF SYSTEM ROBUSTNESS
Substituting (26) into (25), it holds that

$$H$$
$$= \dot{V}_3 + \frac{1}{2}(||y||^2 - \gamma^2||w_1||^2 - \gamma^2||w_2||^2)$$

$$= -c_1 e_1^2 - \frac{c_2 e_2^2}{1-p_1} - \frac{c_3 b_3^2}{1-p_2} - [\frac{\gamma w_2}{\sqrt{2}} - \frac{b_3/(1-p_2)}{\sqrt{2}\gamma}]^2$$

$$- [\frac{\gamma w_1}{\sqrt{2}} - \frac{(\hat{\theta}+c_1+c_2/1-p_1)w_1/(1-p_2)k_1\sin(x_1+\delta_0)}{\sqrt{2}\gamma}]^2$$

$$\leq 0 \tag{27}$$

TABLE 1. Parameters of the FESR.

PARAMETERS	Value/unit
Rated power P_N	2 MW
Rotor blade radius R	45 m
Wind speed v	12 m/s
Direct axis steady reactance X_d	1.52 p.u.
Direct axis transient reactance X_d'	0.152 p.u.
Direct axis transient time constant T_d'	10 s
Reactance of transformer X_T	0.115 p.u.
The moment of inertia H	5.9 s
Infinite bus voltage U_s	1.0 p.u.

According to L_2 gain control, the storage function of the system is

$$V(x) = 2V_3 \quad (28)$$

By integrating both sides of (26) and combining (27), it holds that

$$V(x(t) - x(0)) \le \int_0^t (\gamma^2 ||w_1||^2 + \gamma^2 ||w_2||^2 - ||y||^2) dt \quad (29)$$

From (29), it can be seen that system (13) has L_2 gain from the disturbance to its output, which proves that the designed control method can ensure that the FESR system has the robust disturbance suppression capability. Simulation studies are conducted in the following section to show the effectiveness of the designed controller.

IV. SIMULATION RESULTS AND DISCUSSION

In this section, to prove the effectiveness of the proposed IARC, the low voltage ride-through capability of the FESR under the grid symmetrical and unsymmetrical fault conditions is tested through the simulation of a 2 MW FESR wind power generation system. Additionally, the simulation results of the proposed IARC are compared with the predictive fuzzy PID (PFPID) control as introduced in [41] under the grid symmetrical and unsymmetrical fault. For grid symmetrical faults, two different conditions are considered, i.e., 50% voltage dip and 80% voltage dip. For asymmetrical condition, single-phase ground fault is considered, which assume to occur for 625 milliseconds. The FESR parameters are listed in Table 1.

The parameters in traditional PID control are as follows: $K_p = 6.8$, $K_i = 12.6$, $K_d = 49$.

The parameters in ARC are as follows: $q_1 = 0.4$, $q_2 = 0.6$, $p_1 = 0$, $p_2 = 0$, $c_1 = 5$, $c_2 = 2$, $c_3 = 1.2$, $w_1 = 0.2$, $w_2 = 0.3$, $\rho = 1$, $\gamma = 0.8$.

The parameters in IARC are as follows: $q_1 = 0.4$, $q_2 = 0.6$, $p_1 = 0.25$, $p_2 = 0.45$, $c_1 = 5$, $c_2 = 2$, $c_3 = 1.2$, $w_1 = 0.2$, $w_2 = 0.3$, $\rho = 1$, $\gamma = 0.8$.

A. THE PERFORMANCE ANALYSIS OF LVRT DURING SYMMETRICAL FAULT

1) VOLTAGE DIP TO 50%

The voltage at the point of common coupling (PCC) is decreased to 50% at 0.3 seconds, which persists for

(a) Voltage at PCC

(b) Active power

(c) The rotor speed of the generator
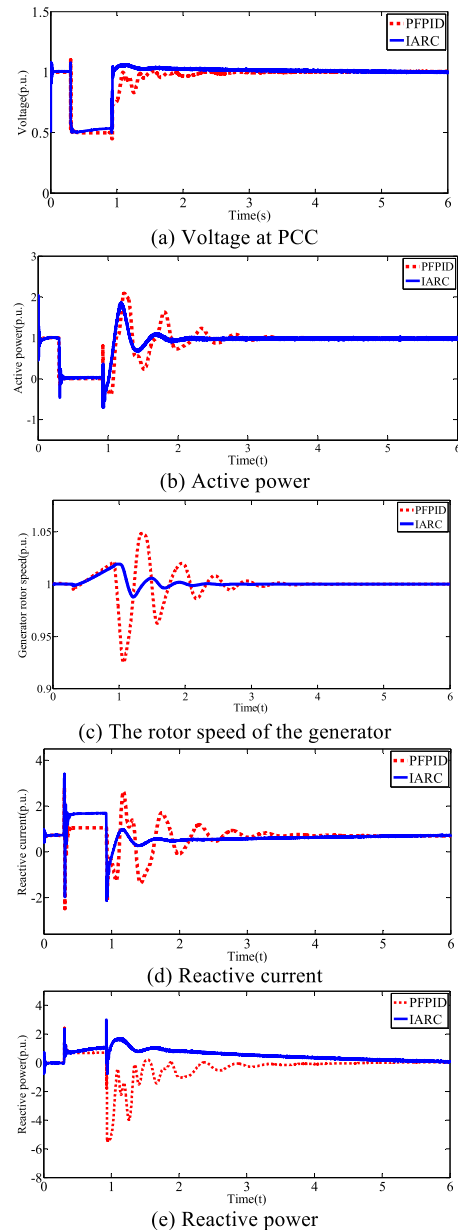
(d) Reactive current

(e) Reactive power

FIGURE 5. Simulation results of LVRT during symmetrical fault for a voltage dip of 50%.

625 milliseconds. The simulation results of the three-phase short circuit fault are obtained from IARC and PFPID control. The voltage at PCC, active power, rotor speed of the generator, reactive current and reactive power are plotted in Fig. 5 (a) to (e), respectively.

As can be seen from Fig. 5(a), the voltage at PCC has transient oscillation and settles at 3.2 seconds using PFPID control, and in the case of using IARC, the voltage at PCC settles at 2.6 seconds, i.e., the transition time of the voltage at PCC is reduced using IARC. As can be seen from Fig. 5(b), the active power peak appears on the time of fault removal, using PFPID control is 2.1 p.u., and using IARC is 1.8 p.u.. Besides, the active power settles at 3.3 seconds using PFPID control and using IARC is 2.2 seconds. It can be found that
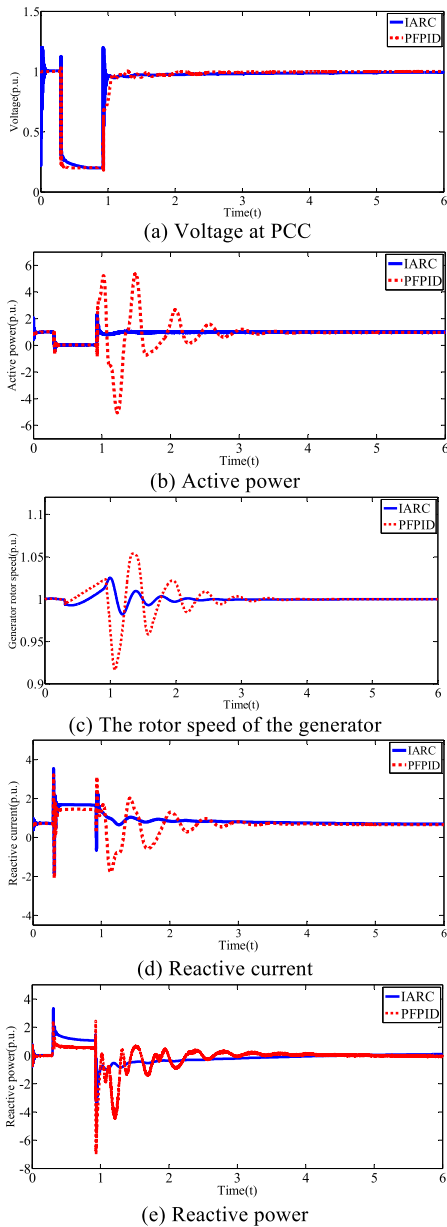
(a) Voltage at PCC

(b) Active power

(c) The rotor speed of the generator

(d) Reactive current

(e) Reactive power

FIGURE 6. Simulation results of LVRT during symmetrical fault for a voltage dip of 80%.

FIGURE 7. Simulation results of LVRT with PFPID during single-phase ground fault.

2) VOLTAGE DIP TO 80%

The voltage at the PCC is decreased to 80%, so the voltage on the grid goes drops to 0.2 p.u.. The fault's duration is 625 milliseconds. The simulation results are obtained for a different method. The voltage at PCC, active power, rotor speed of the generator, reactive current and reactive power are plotted in Fig. 6 (a) to (e), respectively.

Similar to the condition of the voltage dip of 50%, compared with PFPID control, the proposed IARC has a shorter transition time for the voltage at PCC, active power, and generator rotor speed. Meanwhile, the active power peak and generator rotor speed are less, which shows that using IARC can reduce the active impact on the FESR wind power system. Besides, the settling time of reactive current and reactive power is shorter and the peak value of reactive current and reactive power is larger using IARC, which can provide more reactive support for the FESR system. Therefore, it can be concluded that the proposed IARC can improve the LVRT performance of FESR, and have better transient stability and robustness for the FESR wind power system.

B. THE PERFORMANCE ANALYSIS OF LVRT DURING ASYMMETRICAL FAULT

Single-phase ground fault occurs on the transmission line at time 0.3 seconds, and the fault's duration is 625 milliseconds. Fig. 7 shows the simulation results using the conventional ARC, and Fig. 8 shows the simulation results using the proposed IARC. The simulation results of voltage, active power, rotor speed of the generator and reactive power at PCC are plotted in Figures 7 and 8, respectively.

Single-phase ground fault belongs to an asymmetrical fault, and the most important difference with the symmetrical faults is that the negative-sequence current component and DC component are generated in the stator current. Due to the interaction of the positive sequence, the negative sequence and the transient DC component in the stator and rotor currents, the active and reactive power will contain a series of

the peak and the transition time of active power using IARC is less than PFPID control. As can be seen from Fig. 5(c), when using PFPID control and IARC, the generator rotor speed peak is 1.048 p.u. and 1.02 p.u. respectively, and the transition time is 3.7 seconds and 2 seconds. Using IARC is more conducive to the rapid recovery of generator speed after fault is removed. As can be seen from Fig. 5(d), the reactive current peak using PFPID control is 2.8 p.u. and using IARC is 3.4 p.u.. Besides, using PFID control, the reactive power value of the continuous injection system is 1 p.u. and using IARC is 1.8 p.u. Similarly, as can be seen from Fig. 5(e), compared with PFPID control, using IARC can provide more reactive power to the system and is more helpful in recovering the voltage at PCC.
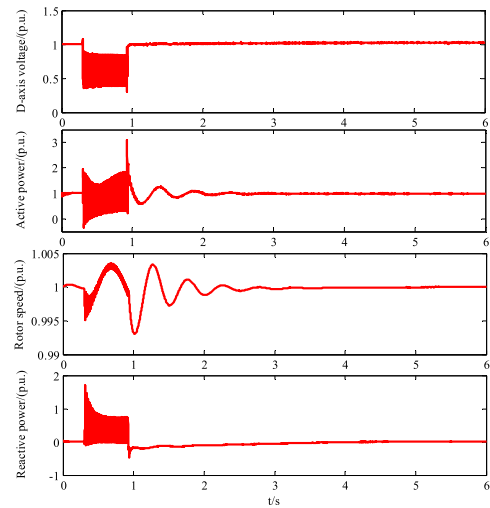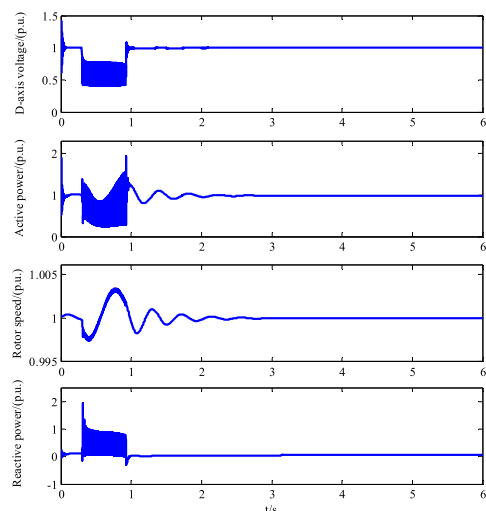
FIGURE 8. Simulation results of LVRT with IARC during single-phase ground fault.

harmonic components. As shown in Fig. 7, in the case of using the PFPID, the transient oscillation amplitude of the d-axis voltage at PCC is 0.9p.u., the reactive power peak is 3.1 p.u., the generator rotor speed settles at 3.8 seconds, and the reactive power peak is 1.8 p.u.. Similarly, as shown in Fig. 8, in the case of using the proposed IARC, the oscillation amplitude of the d-axis voltage at PCC is 0.7 p.u., and the active power peak is 1.8 p.u., which are less than using ARC. The generator rotor speed settles at 2.8 seconds, which shortened by 1 second. The reactive power peak is 2.1 p.u., which is more conducive to the rapid recovery of the grid voltage than using PFPID.

V. CONCLUSION

This paper proposed an LVRT method based on improved adaptive robust control for the FESR. The proposed control method is simulated and compared with the PFPID control by the simulation model of FESR. More importantly, the error compensation term and additional control variable are considered in the design process of the improved adaptive robust controller, which can promote the steady speed of the variables. Furthermore, the improved adaptive robust control can bring smaller oscillation amplitude and shorter settling time, and improve the dynamic response speed of the EESG and the LVRT performance of the FESR during the grid fault. Finally, due to the external disturbance, the non-linearity of the system and the uncertainty of the generator parameters are taken together into consideration in the improved adaptive robust controller. In the simulation results, it can be seen that the proposed control method is more effective in improving the transient stability and robustness of the FESR system during the grid voltage dip.

REFERENCES

[1] Z. Din, J. Zhang, Y. Zhu, Z. Xu, and A. El-Naggar, "Impact of grid impedance on LVRT performance of DFIG system with rotor crowbar technology," *IEEE Access*, vol. 7, pp. 127999–128008, 2019.

[2] R. A. J. Amalorpavaraj, P. Kaliannan, S. Padmanaban, U. Subramaniam, and V. K. Ramachandaramurthy, "Improved fault ride through capability in DFIG based wind turbines using dynamic voltage restorer with combined feed-forward and feed-back control," *IEEE Access*, vol. 5, pp. 20494–20503, 2017.

[3] J. López, P. Sanchis, X. Roboam, and L. Marroyo, "Dynamic behavior of the doubly fed induction generator during three-phase voltage dips," *IEEE Trans. Energy Convers.*, vol. 22, no. 3, pp. 709–717, Sep. 2007.

[4] J. Lopez, E. Gubia, E. Olea, J. Ruiz, and L. Marroyo, "Ride through of wind turbines with doubly fed induction generator under symmetrical voltage dips," *IEEE Trans. Ind. Electron.*, vol. 56, no. 10, pp. 4246–4254, Oct. 2009.

[5] R. Hirawata and T. Kai, "Study of low-voltage ride-through performance for wind power generation with doubly fed induction generator," *Electr. Eng. Jpn.*, vol. 185, no. 1, pp. 17–26, Oct. 2013.

[6] M. I. Mosaad, "Model reference adaptive control of STATCOM for grid integration of wind energy systems," *IET Electr. Power Appl.*, vol. 12, no. 5, pp. 605–613, May 2018.

[7] G. Wen, Y. Chen, Z. Zhong, and Y. Kang, "Dynamic voltage and current assignment strategies of nine-switch-converter-based DFIG wind power system for low-voltage ride-through (LVRT) under symmetrical grid voltage dip," *IEEE Trans. Ind. Appl.*, vol. 52, no. 4, pp. 3422–3434, Jul. 2016.

[8] M. L. Shanoob, K. Iqbal, and A. Al-Maliki, "Wind turbine transient response and fault ride-through improvements with optimal control," *Int. Trans. Electr. Energy Syst.*, vol. 27, no. 11, p. e2412, Nov. 2017.

[9] P. M. Tripathi, S. S. Sahoo, and K. Chatterjee, "Enhancement of low-voltage ride through of wind energy conversion system using superconducting saturated core fault current limiter," *Int. Trans. Electr. Energy Syst.*, vol. 29, no. 4, p. e2798, 2019.

[10] K. Benyahia, A. Mezouar, and L. Boumediene, "Reliability and performance improvement of double-fed induction generator-based wind energy conversion system," *Int. J. Model., Identificat. Control*, vol. 28, no. 4, pp. 370–382, 2017.

[11] C. Rahmann, H.-J. Haubrich, A. Moser, R. Palma-Behnke, L. Vargas, and M. B. C. Salles, "Justified fault-ride-through requirements for wind turbines in power systems," *IEEE Trans. Power Syst.*, vol. 26, no. 3, pp. 1555–1563, Aug. 2011.

[12] M. I. Mosaad, A. Abu-Siada, and M. F. El-Naggar, "Application of superconductors to improve the performance of DFIG-based WECS," *IEEE Access*, vol. 7, pp. 103760–103769, 2019.

[13] G. P. Serb, I. P. Serb, A. Campeanu, S. Degeratu, and A. Petrisor, "Study of the sudden symmetrical short-circuit using the mathematical models of the synchronous machine and the numerical methods," in *Proc. 13th Int. Power Electron. Motion Control Conf.*, Sep. 2008, pp. 893–898.

[14] M. Poller, "Grid compatibility of wind generators with hydro-dynamically controled gearbox with German grid codes," DIgSILENT GmbH, Gomaringen, Germany, Draft Rep., Aug. 2010.

[15] B. Rabelo, W. Hofmann, M. Tilscher, and A. Basteck, "Voltage regulator for reactive power control on synchronous generators in wind energy power plants," in *Proc. NORPIE*, Trondheim, Norway, 2004, pp. 1–6.

[16] H. Müller, M. Poeller, A. Basteck, M. Tilscher, and J. Pfister, "Grid compatibility of variable speed wind turbines with directly coupled synchronous generator and hydro-dynamically controlled gearbox," in *Proc. WIW*, Stockholm, Sweden, 2006, pp. 307–315.

[17] J. Wang, "Research on the low-voltage ride-through capability of wind synchronous generator with hydro-dynamically controlled gearbox," *Electr. Drive Automat.*, vol. 38, no. 3, pp. 1–8, Mar. 2016.

[18] G. Kenné, R. Goma, H. Nkwawo, F. Lamnabhi-Lagarrigue, A. Arzandé, and J. C. Vannier, "An improved direct feedback linearization technique for transient stability enhancement and voltage regulation of power generators," *Int. J. Electr. Power Energy Syst.*, vol. 32, no. 7, pp. 809–816, Sep. 2010.

[19] R. L. A. Ribeiro, C. M. S. Neto, F. B. Costa, T. O. A. Rocha, and R. L. Barreto, "A sliding-mode voltage regulator for salient pole synchronous generator," *Electr. Power Syst. Res.*, vol. 129, pp. 178–184, Dec. 2015.

[20] A. Colbia-Vega, J. de León-Morales, L. Fridman, O. Salas-Peña, and M. T. Mata-Jiménez, "Robust excitation control design using sliding-mode technique for multimachine power systems," *Electric Power Syst. Res.*, vol. 78, no. 9, pp. 1627–1634, Sep. 2008.

[21] T. K. Roy, M. A. Mahmud, W. Shen, and A. M. T. Oo, "Nonlinear adaptive excitation controller design for multimachine power systems with unknown stability sensitive parameters," *IEEE Trans. Control Syst. Technol.*, vol. 25, no. 6, pp. 2060–2072, Nov. 2017.

[22] J. Hao, C. Chen, L. Shi, and J. Wang, "Nonlinear decentralized disturbance attenuation excitation control for power systems with nonlinear loads based on the Hamiltonian theory," *IEEE Trans. Energy Convers.*, vol. 22, no. 2, pp. 316–324, Jun. 2007.

[23] T. Shen, S. Mei, Q. Lu, W. Hu, and K. Tamura, "Adaptive nonlinear excitation control with L_2 disturbance attenuation for power systems," *Automatica*, vol. 39, no. 1, pp. 81–89, Jan. 2003.

[24] J. Cai, C. Wen, H. Su, Z. Liu, and L. Xing, "Adaptive backstepping control for a class of nonlinear systems with non-triangular structural uncertainties," *IEEE Trans. Autom. Control*, vol. 62, no. 10, pp. 5220–5226, Oct. 2017.

[25] K. Wang, D. Gan, H. Xin, and Y. Ni, "Non-linear robust adaptive excitation controller design in power systems based on a new back-stepping method," *IET Control Theory Appl.*, vol. 4, no. 12, pp. 2947–2957, Dec. 2010.

[26] L.-Y. Sun, S. Tong, and Y. Liu, "Adaptive backstepping sliding mode H_∞ control of static var compensator," *IEEE Trans. Control Syst. Technol.*, vol. 19, no. 5, pp. 1178–1185, Sep. 2011.

[27] P. Wu, Q.-Y. Wang, and X.-Y. Feng, "Automatic train operation based on adaptive terminal sliding mode control," *Int. J. Autom. Comput.*, vol. 12, no. 2, pp. 142–148, Apr. 2015.

[28] Q. Su, W. Quan, G. Cai, and J. Li, "Improved adaptive backstepping sliding mode control for generator steam valves of non-linear power systems," *IET Control Theory Appl.*, vol. 11, no. 9, pp. 1414–1419, Jun. 2017.

[29] Q. Su, W. Quan, W. Quan, G. Cai, and J. Li, "Improved robust adaptive backstepping control approach on STATCOM for non-linear power systems," *IET Gener., Transmiss. Distrib.*, vol. 11, no. 13, pp. 3428–3437, Sep. 2017.

[30] Q. Su, F. Dong, and J. Li, "Improved nonlinear robust adaptive backstepping controller design for generator excitation systems," *IEEE Access*, vol. 7, pp. 83187–83197, 2019.

[31] Z. Gu, C. Zhu, T. Shao, and W. Wang, "Adaptive L_2 excitation control with K class functions and additional control variable," *Control Theory Appl.*, vol. 33, no. 2, pp. 257–264, 2016.

[32] Z. Gu, C. Zhu, and T. Shao, "Back-stepping optimal L_2-gain control with rapid adaptation of uncertain parameters," *Syst. Eng. Electron.*, vol. 38, no. 8, pp. 1909–1916, 2016.

[33] T. K. Roy, M. A. Mahmud, and A. M. T. Oo, "Robust adaptive backstepping excitation controller design for higher-order models of synchronous generators in multimachine power systems," *IEEE Trans. Power Syst.*, vol. 34, no. 1, pp. 40–51, Jan. 2019.

[34] H. Lomei, D. Sutanto, K. M. Muttaqi, and A. Alfi, "An optimal robust excitation controller design considering the uncertainties in the exciter parameters," *IEEE Trans. Power Syst.*, vol. 32, no. 6, pp. 4171–4179, Nov. 2017.

[35] L. Pengfei and W. Wang, "Principle, structure and application of advanced hydrodynamic converted variable speed planetary gear (Vorecon and Windrive) for industrial drive and wind power transmission," in *Proc. Int. Conf. Fluid Power Mechatronics*, Beijing, China, Aug. 2011, pp. 839–843.

[36] H. Dong, S. Li, L. Cao, and H. Li, "Voltage and reactive power control of front-end speed controlled wind turbine via h strategy," *Telkomnika Indonesian J. Electr. Eng.*, vol. 11, no. 8, pp. 4190–4199, 2013.

[37] S. M. Tripathi, A. N. Tiwari, and D. Singh, "Grid-integrated permanent magnet synchronous generator based wind energy conversion systems: A technology review," *Renew. Sustain. Energy Rev.*, vol. 51, pp. 1288–1305, Nov. 2015.

[38] R. M. Linus and P. Damodharan, "Maximum power point tracking method using a modified perturb and observe algorithm for grid connected wind energy conversion systems," *IET Renew. Power Gener.*, vol. 9, no. 6, pp. 682–689, Aug. 2015.

[39] H. H. H. Mousa, A.-R. Youssef, and E. E. M. Mohamed, "Model predictive speed control of five-phase permanent magnet synchronous generator-based wind generation system via wind-speed estimation," *Int. Trans. Electr. Energy Syst.*, vol. 29, no. 5, p. e2826, May 2019.

[40] F. Golnary and H. Moradi, "Design and comparison of quasi continuous sliding mode control with feedback linearization for a large scale wind turbine with wind speed estimation," *Renew. Energy*, vol. 127, pp. 495–508, Nov. 2018.

[41] J. Zou, Y. C. Yang, and J. Zhu, "Design of grey model based predictive controllers and its application," *Proc. CSEE*, vol. 22, no. 9, pp. 12–14, 2002.

HAIYING DONG was born in Lintong, China, in 1966. He received the B.S. degree from Beihang University, Beijing, China, in 1989, the M.S. degree from Lanzhou Jiaotong University, Lanzhou, China, in 1998, and the Ph.D. degree from Xi'an Jiaotong University, Xi'an, China, in 2003. He is currently a Professor with Lanzhou Jiaotong University. His research interests include the optimization and intelligent control of power systems, and optimal control of renewable energy generation.

NINGNING CHEN received the B.S. degree in electrical engineering from Lanzhou Jiaotong University, Lanzhou, China, in 2016, where she is currently pursuing the M.S. degree. Her research interest includes the optimal control of renewable energy generation.

XIAOQING LI was born in Wuwei, China, in 1986. She received the B.S. degree in automation and the M.S. degree in control theory and control engineering from Lanzhou Jiaotong University, Lanzhou, China, in 2010 and 2013, respectively, where she is currently pursuing the Ph.D. degree in traffic equipment detection and control engineering. Since 2013, she has been a Teacher with the School of Electrical Engineering, Lanzhou Institute of Technology. Her research interests include optimal operation and intelligent control of power systems, and optimal control of new energy generation.

HONGWEI LI was born in Lintao, China, in 1981. He received the B.S. degree in automation and the M.S. degree in traffic information engineering and control from Lanzhou Jiaotong University, Lanzhou, China, in 2003 and 2009, respectively, where he is currently pursuing the Ph.D. degree in traffic information engineering and control. Since 2003, he has been a Teacher with the School of Automation and Electrical Engineering, Lanzhou Jiaotong University. His research interests include optimal operation and intelligent control of power systems, and optimal control of new energy generation.

• • •